Journal of Thermal Analysis and Calorimetry
https://doi.org/10.1007/s10973-025-14605-x

Method of obtaining dual-phase-lag times in aggregate porous materials with a nonhomogeneous inner structure

A. Massaguer[1] · M. Teixidor[2] · M. Leroy[3] · J. Goeminne[3] · J. J. Suñol[4] · E. Massaguer[1]

Received: 6 May 2024 / Accepted: 21 July 2025

Abstract

When working with porous non-Fourier heat conduction materials under the dual-phase-lag model, it becomes necessary to find out the values of the relaxation (τ_q) and thermalization (τ_T) times. In this article, we propose an experimental method to obtain these lagging times for aggregated carbon nanotubes (CNTs). The method, which can be used for any other material, consists of applying a transient heat pulse at one side of the specimen while registering the temperature–time curves at multiple points along it. The remaining faces of the specimen are thermally isolated. Then, an analytical model incorporating these boundary conditions is executed iteratively, varying the lagging times, to minimize the difference between the experimental and theoretical curves. Finally, the best fitting curve gives the best combination of τ_q and τ_T values. We also present the evolution of the lagging values along the specimen's thickness in a CNT aggregate.

Keywords non-Fourier heat conduction · Dual-phase-lag model · Lagging times · Porous media · Relaxation and thermalization times · Method

Introduction

When studying transient heat conduction through non-Fourier materials, some of them clearly present a strong deviation from Fourier heat conduction due to the finite speed of the thermal wave [1]. In the case of aggregate porous materials with a nonhomogeneous inner structure, the thermal wave is influenced by the multiple cavities inside the material, the contact points in which the heat is transferred between the aggregate particles, among other factors, and the thermal non-equilibrium between particles and interstitial air. Heat can only move forward following the tortuous path around the internal pores. Such behaviour is of great interest in a lot of potential technical and engineering applications like thermoelectric generation, where temperature and heat flux can be time-uncoupled leading to conversion efficiency improvements.

In order to take into consideration this finite thermal wave speed, several theories like phonon dynamics, phonon hydrodynamics, thermomass theory, and extended nonlocal theories have been proposed. The latest, based on the non-equilibrium thermodynamics and the micro–macro interactions of heat carriers lead to, among other theories, the dual-phase-lag (DPL) model [1–3]. This model, in contrast to classical Fourier law, considers the possibility of temperature gradient and heat flux to occur at different times. With this aim, the DPL model incorporates two lagging values, the relaxation (τ_q) and the thermalization (τ_T) times, which represent the delay of the temperature gradient and the heat flux, respectively.

In our recent research, in which we used the DPL model to analyse the behaviour of porous non-Fourier thermoelectric materials, more precisely carbon nanotubes (CNT), we found the necessity to quantify these delays. Observing the existing literature, multiple articles can be found about the DPL model. Most of them are related to novel mathematical findings based on the DPL model [4–8] and hyperbolic

✉ E. Massaguer
eduard.massaguer@udg.edu

[1] Department of Mechanical Engineering and Industrial Construction, University of Girona, C. Universitat de Girona 4, 17003 Girona, Spain

[2] Computer Applications in Science and Engineering, Barcelona Supercomputing Center, Plaça Eusebi Güell 1-3, 08034 Barcelona, Spain

[3] Odisee University College Technologiecampus Gent, Gebroeders De Smetstraat 1, 9000 Gent, Belgium

[4] Department of Physics, University of Girona, C. Universitat de Girona 4, 17003 Girona, Spain

Published online: 09 September 2025

model for heat conduction (HHC) proposed by Cattaneo and Vernotte [9, 10], and make use of fictitious lagging times to evaluate its impact on different parameters.

When studying transient heat conduction through non-Fourier materials, some of them clearly present a strong deviation from Fourier heat conduction due to the finite speed of the thermal wave [1]. In the case of aggregate porous materials with a nonhomogeneous inner structure, the thermal wave is influenced by the multiple cavities inside the material, the contact points in which the heat is transferred between the aggregate particles, among other factors, and the thermal non-equilibrium between particles and interstitial air. Heat can only move forward following the tortuous path around the internal pores. Such behaviour is of great interest in a lot of potential technical and engineering applications like thermoelectric generation, where temperature and heat flux can be time-uncoupled leading to conversion efficiency improvements.

In order to take into consideration this finite thermal wave speed, several theories like phonon dynamics, phonon hydrodynamics, thermomass theory, and extended nonlocal theories have been proposed. The latest, based on the non-equilibrium thermodynamics and the micro–macro interactions of heat carriers lead to, among other theories, the dual-phase-lag (DPL) model [1–3]. This model, in contrast to classical Fourier law, considers the possibility of temperature gradient and heat flux to occur at different times. With this aim, the DPL model incorporates two lagging values, the relaxation (τ_q) and the thermalization (τ_T) times, which represent the delay of the temperature gradient and the heat flux, respectively.

In our recent research, in which we used the DPL model to analyse the behaviour of porous non-Fourier thermoelectric materials, more precisely carbon nanotubes (CNT), we found the necessity to quantify these delays. Observing the existing literature, multiple articles can be found about the DPL model. Most of them are related to novel mathematical findings based on the DPL model [4–8] and hyperbolic model for heat conduction (HHC) proposed by Cattaneo and Vernotte [9, 10], and make use of fictitious lagging times to evaluate its impact on different parameters.

However, more applied studies require to be aware of these values, and that's why some authors focused their work on performing experiments to obtain realistic lagging times. In [11], authors carried out several experiments on a porous material heated by a microsecond laser pulse with the aim to compare theoretical and experimental results. In [12], author conducted experiments on casted sand to determine whether diffusion or wave models can describe the heat propagation. Although semi-realistic lagging values were found, authors spotted them manually adjusting the relaxation time to fit the experimental results. However, results show that neither the HHC nor the diffusion model can properly describe the heat propagation. This failure is explained by the absence of modelling of the microstructural interaction effect in the fast-transient process, and the deviation of HCC and diffusion model increase when the transient time becomes short. Based on this, Tzou achieved much better results using the DPL model [1]. In this study, a method to extract the DPL lagging times is described based on minimizing the difference in the state-space of τ_T and τ_q between experimental data and the theoretical model. Although this work describes a perfectly valid method, it lacks experimental instructions about the setup configuration, or how thermal diffusivity and conductivity are calculated.

Roetzel et al. suggested an experimental method to determine thermal diffusivity and the relaxation time using temperature oscillations [13]. Experimental relaxation time values of sand, $NaHCO_3$, and processed meat, were found and compared to other previous studies [7, 14–16]. However, this study focused only on the use of HHC model. In addition, the complexity of the experimental setup proposed was remarkable, with two thermoelectric modules, one at each side of the specimen, operated under thermal oscillations and thermally connected to a thermostatic bath. In [14], authors performed a study to investigate the hyperbolic behaviour of sand. They make use of a transient hot wire setup to capture the temperature evolution of moist sand at different locations. Other studies [15, 16], that make use of biological tissues as the heat conduction substrate, also extract the relaxation times experimentally. Other articles quantify the phase lag specifically in CNT [19, 20]. However, once more, they are based only on the HHC model.

Liang et al. [17] perform a study of transient heat conduction in sand based on the results of Kaminski et al. [7]. Authors use DPL model to obtain relaxation and thermalization times by best fitting the experimental data. In [18], Najibi et al. used experimental results of [12] to obtain DPL lagging times. However, none of the mentioned studies describe the experimental method to properly extract these values.

Consequently, we realized the lack of an experimental setup and method to obtain the DPL lagging values. That is one of the reasons why we decided to develop a setup and an experimental method applying a transient heat pulse and obtaining temperature–time curves. Then, multiple theoretical curves are calculated using the DPL model for different lagging time ranges and combinations. Finally, all the theoretical DPL curves are compared with the experimental one to find the best fitting DPL curve and subsequently finding the best fitting τ_T and τ_q time values. For the method and the setup, we have taken some inspiration in [1].

In addition, our work includes a comprehensive description of the experimental setup and methodology, including procedures to measure thermal diffusivity and conductivity—critical parameters in this type of analysis. We validated

the method using a CNT aggregate sample and present the resulting data. The conclusions include a discussion of methodological improvements to enhance the accuracy and reliability of the extracted parameters.

Recent literature supports the importance of such comprehensive modelling approaches. For instance, models incorporating thermal non-equilibrium and dual-phase lag considerations have been applied to complex domains such as PCM-based latent heat thermal energy storage systems [19], thermal management of nanofluid-based finned enclosures [20], and the behaviour of hybrid nanofluids under transient conduction [21]. These studies emphasize the growing relevance of advanced heat conduction models not only in microscale porous systems but also in larger-scale engineering applications where classical theories are insufficient.

Methodology

To obtain the relaxation time values, we propose a transient state experiment with the application of heat pulses to the specimen. The methodology consists of obtaining experimental temperature–time curves at multiple positions inside the material, and then compare these curves to a semi-analytical model based on the DPL theory. Then, the best fitting between two curves is found varying systematically the values for τ_T and τ_q. Consequently, the lagging times can be found when the minimum error is achieved.

Mathematical basis

The procedure consists on subjecting the sample material to: i) a heat pulse on one side of the specimen, (1), ii) a thermal isolation on the remaining sides of the specimen, (2), and considering the initial conditions of iii) an uniform initial temperature, (3), and iv) assuming no thermal disturbance in the bed before instrumentation, (4).

$$q = \begin{cases} q \ for \ \ 0 \le t \le t_s \\ 0 \ \ otherwise \end{cases} \tag{1}$$

$$\frac{\partial T(x,t)}{\partial x} \text{at } x = L \tag{2}$$

$$T(x,0) = T_0 \tag{3}$$

$$\frac{\partial T(x,0)}{\partial t} = 0, \ \text{implying } q(x,0) = 0 \tag{4}$$

In this particular case, a solution can be found by applying the Laplace transform to (1), and (2) and using the initial conditions (3) and (4). The transformed solution is

$$\overline{T}(x;p) = D_1 e^{-Ax} + D_2 e^{Ax} \tag{5}$$

where

$$\begin{aligned} D_1 &= \frac{q_b \alpha}{\lambda} \frac{A}{p\left(1 - e^{-2AL}\right)} \\ D_2 &= D_1 e^{-2AL} \\ A &= \sqrt{\frac{p\left(1 + p\tau_q\right)}{\alpha\left(1 + p\tau_T\right)}} \\ q_b &= \frac{q_s\left(1 - e^{-pt_s}\right)}{p} \end{aligned} \tag{6}$$

The inversion of (5) can be found by the Riemann sum approximation as

$$T\left(x,t|\tau_q,\tau_T\right) = \frac{e^{\gamma t}}{t}\left[\frac{\overline{T}(x,\gamma)}{2} + \text{Re}\sum_{n=1}^{N}(-1)^n \overline{T}\left(x;\gamma + \frac{in\pi}{t}\right)\right]_{\tau_q,\tau_T} \tag{7}$$

considering $\gamma t \cong 4.7$ for faster convergence [2, 3, 22, 23].

Then, taking advantage of this semi-analytical solution and choosing an arbitrary pair of τ_q and τ_T, one can calculate the error E between the theoretical local temperature $T_{DPL}\left(x_i,t_i;\tau_q,\tau_T\right)$ at $\left(x_i,t_i\right)$ and the experimental temperature $T_{exp}\left(x_i,t_i\right)$. The error threshold is defined based on average deviation as

$$E_{\text{Th - Ex}}\left(\tau_q,\tau_T\right) = \frac{\sum_{i=1}^{M}\left|T_{DPL}\left(x_i,t_i;\tau_q,\tau_T\right) - T_{exp}\left(x_i,t_i\right)\right|}{M} \tag{8}$$

Then, employing a contour pattern of the error estimate one can determine the values of τ_q and τ_T where the error is minimum.

Experimental setup and procedure

The experimental setup proposed is the one shown in Fig. 1. It consists of a 0.6-mm graphite sheet heater at the centre of the setup. The heater is cut in a pattern, shown in Fig. 2. In this study, a handmade heater is considered for its versatility and simplicity, which could be useful for other researchers. However, a thin commercial heater can also be used.

On each side of the heater, there is the testing material compartment, where the material is poured, with 60 × 60x20 mm dimensions each. The setup is based on a guarded hot plate method where a hot plate is sandwiched

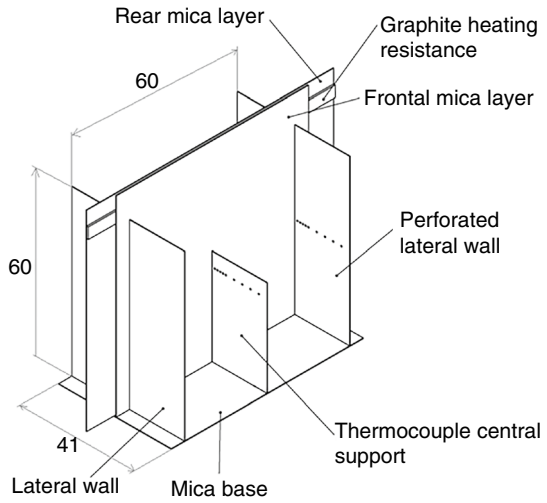

Fig. 1 Isometric drawing of the experimental setup without the external insulation foam. The general measures are also shown. Units in mm

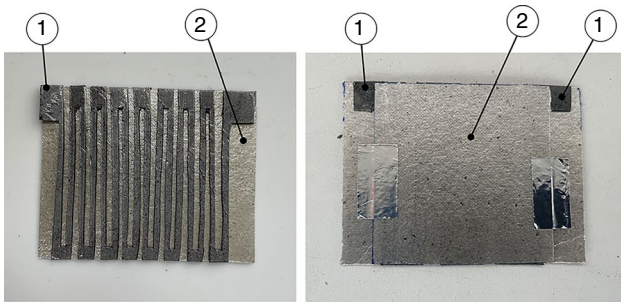

Fig. 2 Image of the heating resistance. Where (1) is the graphite heating resistance and (2) is a mica layer

between two identical samples in order to minimize the heat losses. Ideally, half of the total heat flux induced by the heater will cross each compartment. In order to contain the material, the walls of the compartments are made of a 0.2-mm mica layer, which prevents the electric contact between the material and the graphite heater and at the same time withstands temperatures up to 250ºC. The width and height of the testing compartments are considerably bigger than the thickness, the reason is to grant the insulation of the measuring zone (centre) to minimize the heat losses. In addition, with the same objective, a layer of 20 mm of foam insulation is added to the external faces. All these components mentioned above can be observed in Figs. 1–4.

After the first tests, we realized that for distances far from the heater, temperature measurements differed greatly, more than 30%, from the theory. The reason was that the heat losses were excessively high to be neglected in the experiment. It is important to emphasize that the semi-analytical model is built considering a perfect thermal insulation of the specimen, as Eq. 4 states. Then, in order to overcome this problem, we decided to add a thermal insulation foam around the experimental setup, as shown in Fig. 3.

Before starting the experiments, it is necessary to pour the test material inside both testing compartments. It is important to prevent air cavity formation during the pouring of the material, which could alter the homogeneity of the aggregate material and consequently the heat transport through the material. To prevent this from happening, it is advisable to carefully pour the material followed by a gentile shaking in order to accommodate it.

The proposed experiment starts by generating a heat pulse using the graphite heat resistance. The duration of the heat pulse is controlled using a programmable power source (Keithley 2230) that supplies a precise voltage. Experimental data is gathered using a digital acquisition system (Keithley DAQ 6510). The general experimental setup is shown in Fig. 4. The accuracy of the acquisition system is very high, ± 1.6 mA, ± 2.6 mV and ± 0.2ºC for current, voltage and thermocouple measurements, respectively, so inaccuracies will be neglected.

During the testing, it was necessary to obtain temperature data. In this case, we used 0.25 mm type-K thermocouples because of the fast thermal response needed for this type of transient state experiments. Accuracy of such thermocouples is ± 1.5ºC. The thermocouples were positioned in the middle of one of the two testing compartments. It is important for all the thermocouple tips to be at the same plane, and at the middle of the testing cavity. To achieve that, a mica layer with positioning holes was located parallel to the heat flow direction, as it can be seen in Figs. 1 and 3, so the thermocouple tips can lay in the holes, preventing them from moving when the material is

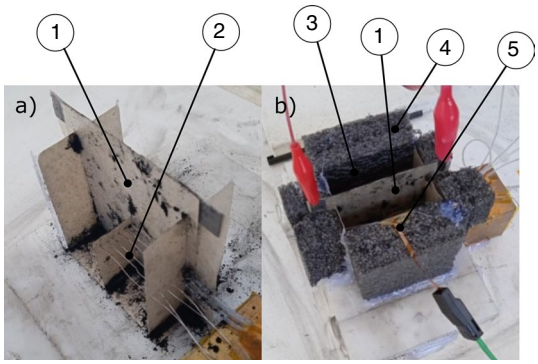

Fig. 3 **a** Image of the experimental setup without the external insulation foam. The general structure of the setup can be observed, as well as the graphite heating resistance, the thermocouples, and some remaining CNTs after the tests. **b** Image of the setup with the external insulation foam. The two testing compartments can be clearly observed. Where (1) is the heater, (2) are the T_0 to T_5 thermocouples, (3) is the CNT aggregate, and (4) is the external insulation

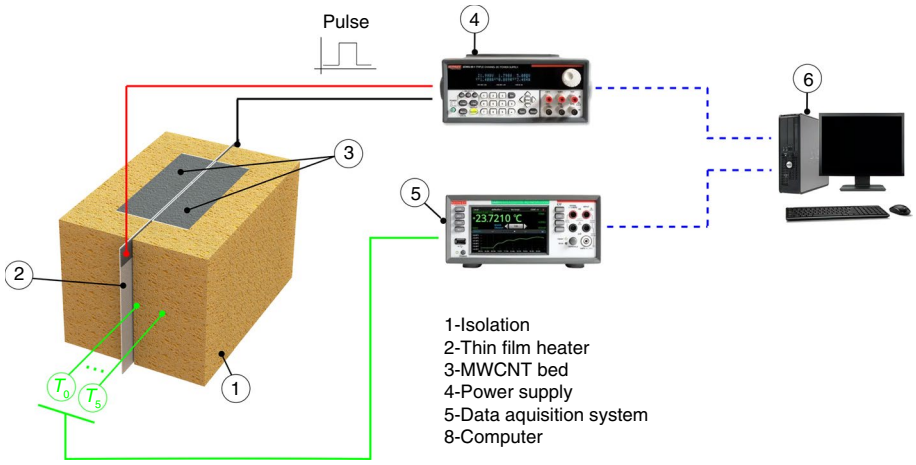

Fig. 4 General scheme of the laboratory setup. Where (1) is the external insulation foam, (2) is the heating resistance, (3) is the CNT aggregate, (4) is the programable power source, (5) is the data acquisition system, and (6) is the computer used to store the data acquired and set the instructions. Note that T_0 to T_5 are 0.25 mm Type-K thermocouples

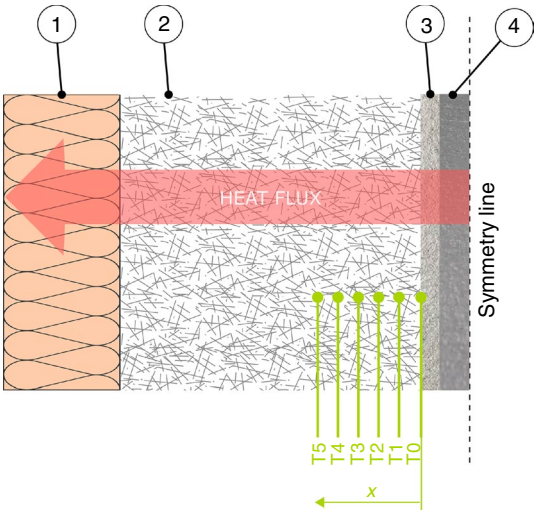

Fig. 5 Diagram of the thermocouples real measured positions. Where (x) is the distance between the temperature point and the mica layer, (1) is an external insulation foam, (2) is the CNT bed, (3) is the mica layer and (4) is the graphite heating resistance

poured and to secure their position. Another set of holes is made in the exact same positions in one of the lateral walls of the testing compartment to allow the thermocouples to exit the compartment. It was essential to precisely measure the distance between each thermocouple tip and the hot face of the heater, as it will be later necessary for the theoretical curve simulations of the DPL model. In this case, 6 thermocouples were installed in the experimental setup, and their final measured positions are the ones shown in Fig. 5. The lagging behaviour is stronger nearby the heat source, so it is advisable to concentrate some temperature sensors closer to the heater. In this study, for pedagogical purposes, we focused only on the region closer to the heater to capture better the lagging behaviour. However, installing temperature sensors further this position will exhibit the decaying evolution of relaxation and thermalization times and the location of the lagging to Fourier diffusion transition point.

It was also necessary to obtain the electrical power supplied to the heat pulse generator. The programmable power source used in this study proportionate this data without requiring supplementary voltage or current metres. It communicates the power measurement directly to the data acquisition system. The thermal power of the heat pulse through one cavity will correspond to the half of the electric power supplied, as only one half goes through one testing compartment where the thermocouples are located. In this method, each compartment is considered homogeneous and identic.

Once the experimental data is obtained, it must be processed in order to be correctly applied to the DPL model. The temperature measurements have been taken in absolute temperature, but for the semi-analytical model described it is required to work with relative temperature referred to the undisturbed initial temperature of the specimen just before the heat pulse was applied. Then, all the temperatures should be relative to the temperature in that instant.

For the theoretical simulated curves, the DPL model equations presented in chapter 3 have been implemented in a MATLAB code. The programme calculates the transient temperature curves for given values of the specific position, thermal conductivity, and diffusivity of the material, power of the heat flow, heat pulse duration, and a range of τ_T and τ_q relaxation times.

The final value of lagging times is unknown, so the procedure is iterative. It starts with an initial guess, let's say both values can vary from 0 to 100 s. Then, the algorithm compares the experimental and theoretical data to find the minimum error. If it is not found in the previously mentioned range, it must be extended until minimum is found. This procedure is further explained in chapter 5.2.

Results and discussion

Determination of thermal conductivity and diffusivity

The thermal conductivity and diffusivity can be extracted using several techniques and laboratory devices. However, for simplicity reasons, these values have been calculated using the Price's method [24]. It is based on the calculation the thermal conductivity and diffusivity from a transient heat conduction experiment. In the experimental setup, a steady-state heat flow is applied to the testing material specimen while the cold side temperature is kept undisturbed.

If the temperature rate of these experiments is small enough, the Fourier law can be satisfied, and the Price's method can be applied.

The temperature difference θ between faces of the specimen is:

$$\theta = \frac{qL}{\lambda}\left[1 - \frac{8}{\pi^2}\sum_{\eta=0}^{\infty}(2\eta+1)^{-2}e^{\frac{-\alpha t\pi^2(2\eta+1)^2}{4L^2}}\right] \tag{9}$$

where q is the constant rate of heat flux input, L is the thickness of the specimen material, t is the time duration in which the heat pulse is applied, and η is the term of the series. If the time values are large enough, all the terms in the time-dependent infinite series in the previous equation can be neglected. Then, after some transformations the expression reduces to

$$\theta = \frac{qL}{\lambda} - \frac{4L^2}{\pi^2\alpha}\frac{\mathrm{d}\theta}{\mathrm{d}t} \tag{10}$$

Finally, thermal conductivity and diffusivity can be determined representing Eq. 10. at the coordinate $(\theta,\mathrm{d}\theta/\mathrm{d}t)$, where $\theta_I = qL/\lambda$ is the ordinate at the origin and the slope $\sigma = -(4L^2)/(\pi^2\alpha)$. Then, λ and α values can be calculated. The representation of Eq. 10 and its least squares fitting line is shown in Fig. 6.

As shown, the least squares fittings obtain a good representation of the results. Following the recommendations in [24], the fitting lines are calculated using the data from a nonlinear fitting of the transient signal using the expression $\theta = \theta_I\left(1 - e^{-\frac{t}{\sigma}}\right)$ instead of using the experimental data directly. This consideration achieves better results because small fluctuations of temperature can be neglected. Finally, Table 1 summarizes the obtained values of λ and α. For these experiments, the averaged values of λ and α are $0.388\,Wm^{-1}K^{-1}$ and $8.45\,10^{-7}m^2s^{-1}$, respectively.

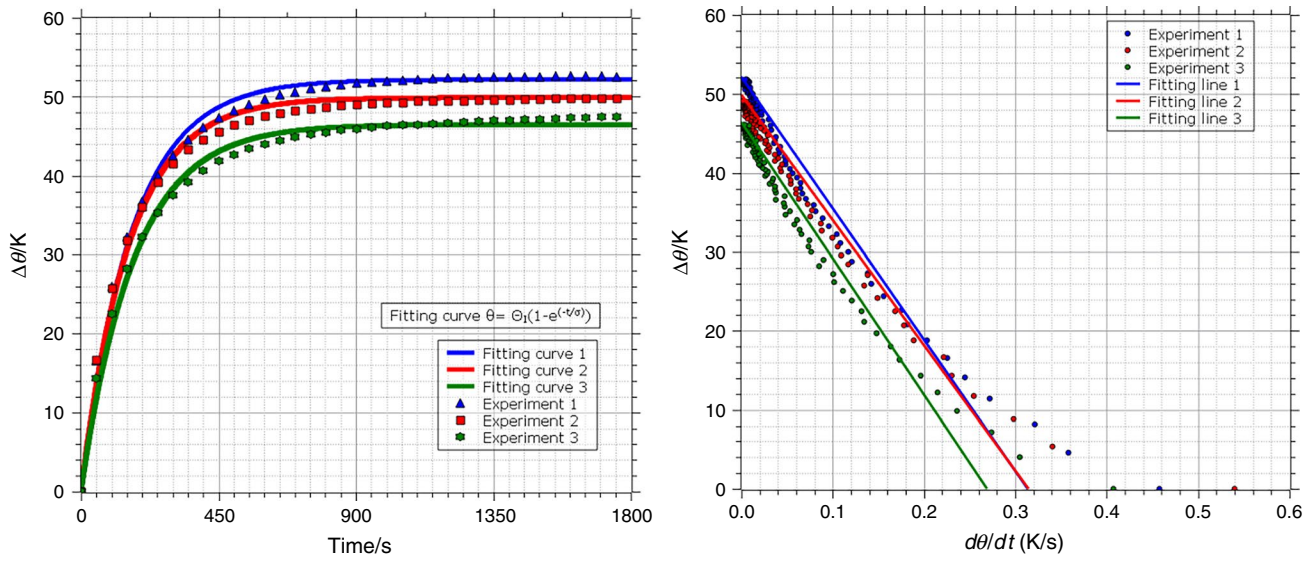

Fig. 6 Least squares fitting lines of the experimental values $(\theta,d\theta/dt)$

Table 1 Calculated values of λ and α using the Price's method

Experiment	t/s	q/Wm^{-2}	L/m	θ_I/K	σ/s	$\lambda/Wm^{-1}K^{-1}$	α/m^2s^{-1}
1	1800	1065.6	0.019	52.2	−166.3	0.388	8.798E−7
2	1800	1027.4	0.019	49.9	−158.6	0.391	9.225E−7
3	1800	987.7	0.019	48.4	−198.8	0.387	7.360E−7

Table 2 Values of thermal conductivity and diffusivity used for the DPL theoretical calculations

Property	Range of values
Thermal conductivity / λ	0.378 – 0.414 W m^{-1} K^{-1}
Thermal diffusivity / α	8.12×10^{-7} – 8.45×10^{-7} m^2s^{-1}

To consider the possible inaccuracies during the determination of these values, the measurement error has been added, the range of the final values used in the theoretical DPL simulations are shown in Table 2.

Determination of lagging values

Once the theoretical DPL values are calculated, the algorithm also calculates the difference between each theoretical temperature–time curves and the experimental ones and displays the cumulative error between curves. When the generated MATLAB programme finishes its tasks, another algorithm has been developed to find which theoretical DPL temperature–time curve fits better with the experimental data. When the error is below the desired threshold the best fitting curve is found, the τ_T and τ_q relaxation time values are consequently determined.

As the final lagging values are unknown, this process is iterative. It starts with an initial guess, considering a given range of each lagging value. If minimum error is found on the range boundaries it means that range must be extended. This procedure must be repeated until minimum error is enclosed in the range of τ_T and τ_q. Once the minimum error is roughly delimited is recommended to make further iterations: narrowing the range of τ_T and τ_q values and increasing the step resolution of each lagging time range.

The exposed setup and method have been used to obtain the relaxation time values for CNTs. The carbon nanotubes used in the experiments are multi-walled (MWCNTs), with an outer diameter of 20–40 nm and a length of 10–30 µm. However, this procedure can be applied to other aggregate materials.

For this study, a heat pulse of 23036 Wm^{-2} for 30 s is applied to the heating resistance. Then, as previously said, is assumed that each compartment will receive half of the total amount.

To properly identify the results, it is useful to represent a 3D plot or a 2D topographic graph with the $E_{Th\,-\,Ex}$ error calculated for each combination of τ_T and τ_q. It helps locating the region where the minimum error is found, see Fig. 7.

In Fig. 7 a, contour plot of the error threshold at T0 is shown. The error between theoretical and experimental temperature–time curves decreases for a particular combination of lagging values. In red, there is the minimum error value

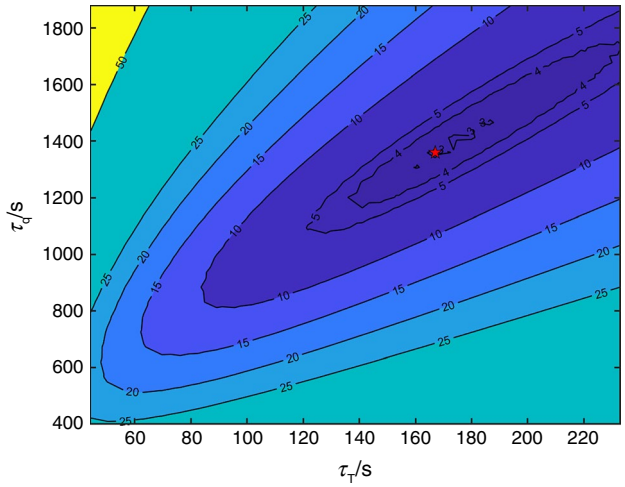

Fig. 7 Contour plot of the error threshold E_{Th-Ex} at T0 considering $t_s=30$ s, $q_s=11518Wm^{-2}$, $L=20$ mm, $\lambda=0.388$ Wm^{-1} K^{-1}, and $\alpha=8.45\times10^{-7}$ m^2s^{-1}

of 2.93% when of $\tau_T = 186.5s$ and $\tau_q = 1465.3s$. How the experimental and theoretical curves fit is shown in Fig. 8.

The locations of each thermocouple are shown in Fig. 5, and the obtained temperature–time curves in experiments and DPL simulations are shown in Fig. 8.

For transient heat transport in MWCNT bed, as demonstrated in Fig. 8, the DPL model yields satisfactory results compared to the experimental data, theoretical, and experimental data match reasonably well.

Table 3 summarizes the lagging time values for each temperature sensor location. In addition, to present the error of the procedure exposed in this study, the error E_{Th-Ex} between the experimental and the theoretical temperature–time curves is also calculated.

To assess the uncertainty associated with the parameters of τ_T and τ_q and obtained through inverse analysis, an error margin of ± 1.5 °C was considered for the experimental temperature measurements. This uncertainty range was applied by considering this range of variation over the measurements. Then, for each adjusted dataset, the inverse fitting procedure was repeated to extract the corresponding values of maximum τ_T and τ_q. The maximum deviations in these parameters, compared to the values obtained from the original experimental data, were then calculated and shown in Table 3. These differences represent the estimated uncertainty in τ_T and τ_q due to measurement errors in temperature. In other words, this analysis evaluates the sensitivity of the extracted parameters to the experimental uncertainty and provides an estimate of the maximum deviation of τ_T and τ_q that can be expected within the bounds of measurement error.

Physically, the lagging response in this type of medium is caused by the finite time required for heat to travel through

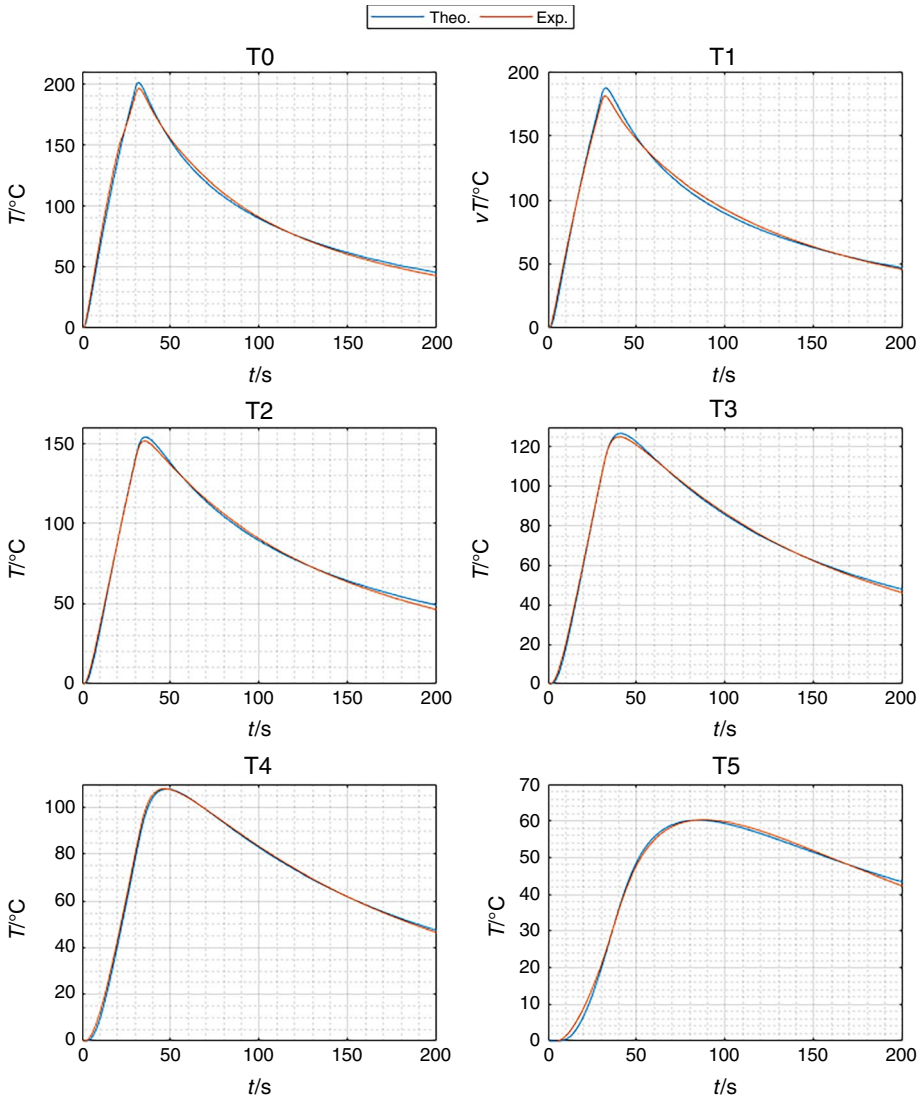

Fig. 8 Graphs of the experimental and DPL theoretical temperature–time curves from T_0 to T_5

Table 3 Ranges for the relaxation time values obtained

	Position / mm	τ_q/ s	τ_T/ s	E_{Th-Ex}/ %	Uncertainity	
					τ_q/ s	τ_T/ s
T0	0	1465.3	186.5	2.93	±11	±5
T1	0.3	1115.6	186.8	2.80	±33	±6
T2	1.3	830. 0	176.5	1.62	±27	±6
T3	1.6	671.3	151.6	1.04	±25	±6
T4	2.2	577.0	134.1	1.18	±21	±5
T5	5.3	345.6	117.0	0.81	±16	±5

the internal pores and to establish a thermal equilibrium between trapped air and MWCNT particles and the wavy conducting path that heat carriers must follow along the solid phase. Lagging times strongly depend on this non-equilibrium, and this is the main cause for the space-dependent phase lags in the near field surrounding the heater. Closer to the heater, lagging values tend to increase greatly, especially the relaxation time, reaching a value of almost 1500 s at 0 mm from the heater. Thermalization time also increases in this direction but at slower rate. On the contrary, the lagging times diminish when departing from the heater. This is due to enough heat carrier collisions leading to a better thermal equilibrium between phases. Both lagging values decay up to a certain point where lagging values reduce to zero and

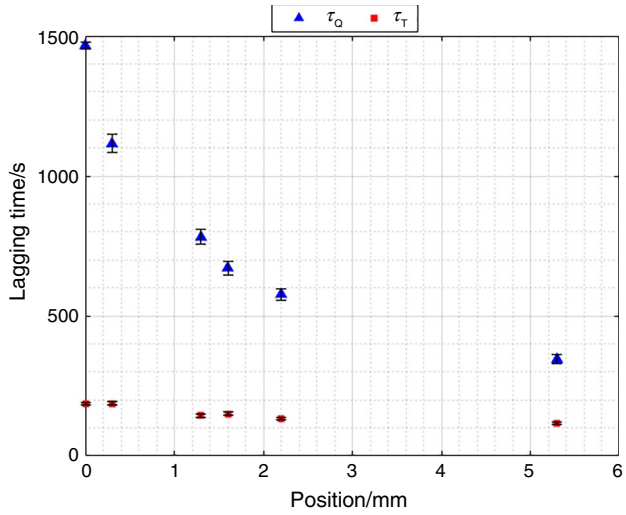

Fig. 9 Graph of the DPL lagging values obtained at different locations with uncertainty bars

the transient response is represented by Fourier diffusion. The purpose of this study was the extraction of the phase lag values in the near field of the heater, where they exhibit larger variations. This is the reason why the location of the lagging frontier has not been found. However, this procedure can be applied to obtain this point and the precedence switching also.

Finally, the lagging time evolution along the specimen for each test carried out is plotted in Fig. 9.

Even DPL lagging values of CNT aggregates are not found in the literature, trends of the lagging values obtained using the methodology presented in this work are in accordance with other studies that employed other materials [1, 25].

Conclusions

We believe the proposed method and setup are valid and can be useful for the scientific community for determining the DPL relaxation time values of aggregate materials.

The obtained lagging times for aggregated CNTs are coherent and are found within the same order of magnitude with other scientific publications mentioned in the introduction [1, 25]. This large lagging behaviour combined with the low thermal conductivity suggest that CNT aggregates could have a potential use to increase the efficiency of thermoelectric generators by using transient heat pulses. Some other studies also refer to this potential application [25–29]. In this scenario, the proposed method and setup could become a very useful tool to characterize the lagging behaviour of these non-Fourier porous materials under transient states.

In this study, the maximum error of this procedure when extracting the lagging times is found to be 2.93%. It is observed that the farthest thermocouples experience a greater deviation with respect to the adiabatic boundary condition of the model. Authors concluded that it is because of the convection heat losses. In order to prove this theory and reduce the convection heat losses, the material was isolated with polyethylene foam plates. The obtained results clearly improved and matched reasonably better. However, authors believe that heat losses would be still noticeable if more temperature sensors had been placed near the far end of the specimen.

While using the method presented in this study, it is capital to ensure a perfect thermal isolation of the system, otherwise the accuracy of lagging times calculated is in great compromise. As a recommendation, it would be advisable to carry out the experiments under vacuum conditions, placing the experimental setup inside a vacuum chamber, as this would reduce the convection heat losses drastically. In case of unavailability of a vacuum chamber, it is recommendable to add a low heat conduction isolation to the surroundings of the specimen. Its thickness is also very important and need to be carefully chosen. Another option is to extend the specimen's length and width and to place temperature sensors in the near field of the heater surface. This will minimize heat losses at the study location.

In case of testing materials with smaller lagging times or under a faster heat pulse, it is recommended to use thin and fast-responsive thermocouples such as special grade type T, R or S, which would grant better precision and improve the temperature readings. It would also be recommended to do a loop back to eliminate possible interferences. In addition, once a preliminary test is performed and the Fourier frontier position determined, for accuracy reasons the use of RTD temperature sensors for locations near and further this frontier is also recommendable. This would allow a better determination of the diffusion frontier location.

This study introduces a reliable and accurate experimental method for determining dual-phase-lag (DPL) relaxation times in aggregated materials such as carbon nanotube (CNT) assemblies. The results align well with previously reported values, confirming the method's validity. The observed combination of large lagging times and low thermal conductivity in CNT aggregates suggests their potential use in improving the efficiency of thermoelectric generators operating under transient heat conditions. The work also highlights the critical role of thermal isolation and offers practical recommendations to minimize experimental error. Overall, this study contributes a practical and replicable tool for characterizing non-Fourier heat conduction in porous materials, advancing both thermal analysis methodologies and the development of energy conversion technologies.

Acknowledgements The project has been co-funded by the Ministry of Science and Innovation through the call of proposals for "Projects oriented towards ecological transition and digital transition" (TED2021-130536A-I00)

Funding Open Access funding provided thanks to the CRUE-CSIC agreement with Springer Nature. Ministerio de Ciencia e Innovación, TED2021-130536A-I00, Eduard Massaguer

References

1. Tzou, D. Y. Macro- to Microscale Heat Transfer: The Lagging Behavior. (Wiley, 2014). https://doi.org/10.1002/9781118818275
2. Tzou DY. The generalized lagging response in small-scale and high-rate heating. Int J Heat Mass Transfer. 1995;38:3231–40. https://doi.org/10.1016/0017-9310(95)00052-B.
3. Tzou DY. Experimental support for the lagging behavior in heat propagation. J Thermophys Heat Transf. 1995;9:686–93. https://doi.org/10.2514/3.725.
4. Shaahmadi F, Mehraban M, Khosravi-Nikou MR. Non-fourier heat conduction with periodic thermal condition for porous fin. Iranian J Sci Technol Trans Mech Eng. 2017;41:209–15. https://doi.org/10.1007/s40997-016-0053-1.
5. Wang L, Wang J. A heat conduction equation for heterogeneous media and its connections to various known equations. Int Commun Heat Mass Transfer. 2021;125:105087. https://doi.org/10.1016/j.icheatmasstransfer.2020.105087.
6. Vadasz P. On the paradox of heat conduction in porous media subject to lack of local thermal equilibrium. Int J Heat Mass Transf. 2007;50:4131–40. https://doi.org/10.1016/j.ijheatmasstransfer.2007.03.017.
7. Kaminski W. Hyperbolic heat conduction equation for materials with a nonhomogeneous inner structure. J Heat Transfer. 1990;112:555–60. https://doi.org/10.1115/1.2910422.
8. Tamma K, Zhou X. Macroscale and microscale thermal transport and thermo-mechanical interactions: some noteworthy perspectives. J Therm Stress. 1998;21:405–49. https://doi.org/10.1080/01495739808956154.
9. Cattaneo C. A form of heat-conduction equations which eliminates the paradox of instantaneous propagation. Comptes Rendus de l'Academie Des Sci. 1958;247:431–3.
10. Vernotte P. Paradoxes in the continuous theory of the heat equation. Comptes Rendus. 1958;246:3154–5.
11. Jiang F. Non-Fourier heat conduction phenomena in porous material heated by microsecond laser pulse. Microscale Thermophys Eng. 2003;6:331–46. https://doi.org/10.1080/10893950290098386.
12. Yunsheng X, Yingkui G, Zengyuan G. Experimental research on transient heat transfer in sand. Acta Mech Sin. 1996;12:39–46. https://doi.org/10.1007/BF02486760.
13. Roetzel W, Putra N, Das SK. Experiment and analysis for non-Fourier conduction in materials with non-homogeneous inner structure. Int J Therm Sci. 2003;42:541–52. https://doi.org/10.1016/S1290-0729(03)00020-6.
14. Graßmann, A., Peters, F. Experimental investigation of heat conduction in wet sand. Heat and Mass Transfer 35, 289–294 (1999). https://doi.org/10.1007/s002310050326
15. Herwig, H., Beckert, K. Experimental evidence about the controversy concerning Fourier or non-Fourier heat conduction in materials with a nonhomogeneous inner structure. Heat and Mass Transfer 36, 387–392 (2000). https://doi.org/10.1007/s002310000081
16. Kumar S, Vedavarz A, Moallemi MK, Mitra K. Experimental Evidence of Hyperbolic Heat Conduction in Processed Meat, 1995. http://heattransfer.asmedigitalcollection.asme.org/.
17. Guo Z, Xu Y, Liang X. Theoretical analysis of transient heat conduction in sand. Sci China Ser A-Math. 1996;39:855–63.
18. Najibi A, Shojaeefard MH. Fourier and time-phase-lag heat conduction analysis of the functionally graded porosity media. Int Commun Heat Mass Transf. 2022;136: 106183. https://doi.org/10.1016/j.icheatmasstransfer.2022.106183.
19. Zheng R, Jiang X, Zhang H. Efficient and accurate spectral method for the time-fractional dual-phase-lag heat transfer model and its parameter estimation. Math Methods Appl Sci. 2020;43:2216–32. https://doi.org/10.1002/mma.6035.
20. Antaki PJ. Electric circuit analogs of first-order dual-phase-lag diffusion. J Comput Nonlinear Dyn. 2025. https://doi.org/10.1115/1.4067256.
21. Lukashchuk SYu. A semi-explicit algorithm for parameters estimation in a time-fractional dual-phase-lag heat conduction model. Modelling. 2024;5:776–96. https://doi.org/10.3390/modelling5030041.
22. Tzou DY, O¨zis¸ik MN, Chiffelle RJ. The lattice temperature in the microscopic two-step model. J Heat Transfer. 1994;116:1034–8. https://doi.org/10.1115/1.2911439.
23. Tzou DY. A unified field approach for heat conduction from macro- to micro-scales. J Heat Transfer. 1995;117:8–16. https://doi.org/10.1115/1.2822329.
24. Price WLV. The calculation of thermal conductivity and thermal diffusivity from transient heating measurements. Build Environ. 1983;18:219–22. https://doi.org/10.1016/0360-1323(83)90029-X.
25. Liu K, Cui S, Kan W, Qi X, Chen C, Hu X. Giant thermal transport phase lagging in CNT aggregates. Nanoscale Microscale Thermophys Eng. 2013;17:236–44. https://doi.org/10.1080/15567265.2013.787569.
26. Liu K, Cui S, Qi X, Chen C, Hu X. Thermal conductivity and thermal transport relaxation time of CNT packed beds, In: Volume 7: Fluids and Heat Transfer, Parts A, B, C, and D, American Society of Mechanical Engineers. 2012. pp. 2725–2729. https://doi.org/10.1115/IMECE2012-87164.
27. Liu K, Li M, Cui S, Hu X. Large thermal transport phase lagging improves thermoelectric efficiency. Appl Phys A Mater Sci Process. 2013;111:477–81. https://doi.org/10.1007/s00339-012-7498-x.
28. Prasher RS, Hu XJ, Chalopin Y, Mingo N, Lofgreen K, Volz S, Cleri F, Keblinski P. Turning carbon nanotubes from exceptional heat conductors into insulators. Phys Rev Lett. 2009;102:1–4. https://doi.org/10.1103/PhysRevLett.102.105901.
29. Wang X, Wang H, Liu B. Carbon nanotube-based organic thermoelectric materials for energy harvesting. Polymers. 2018;10:1196. https://doi.org/10.3390/polym10111196.